Available online at www.sciencedirect.com
ScienceDirect
Journal of Power Sources 168 (2007) 240–250
JOURNAL OF POWER SOURCES
www.elsevier.com/locate/jpowsour

Dynamic behavior of PEM FCPPs under various load conditions and voltage stability analysis for stand-alone residential applications

M. Uzunoglu [1], O.C. Onar [1], M.S. Alam *

Department of Electrical and Computer Engineering, University of South Alabama, 307 University Boulevard North, Mobile, AL 36688-0002, USA

Received 29 December 2006; received in revised form 31 January 2007; accepted 2 February 2007
Available online 27 February 2007

Abstract

In this paper, dynamic behavior and performance of a fuel cell power plant (FCPP) which operates in parallel with a battery bank is tested under classified load conditions, such as mostly resistive, mostly inductive, resistive-inductive and non-linear loads. Thereafter, voltage stability analysis is performed using the dynamic response of the FCPP for stand-alone residential applications. Simulation results are obtained using the MATLAB® and Simulink® software packages, based on the mathematical and dynamic electrical models of the system. Using the experimental results, a validated model has been realized and voltage stability analysis is performed through this model.

Keywords: Fuel cell; Load conditions; PEM FCPP; Reactive power; Stand-alone; Voltage stability

1. Introduction

Fuel cell power plants (FCPPs) are electrochemical devices that convert the chemical energy of a reaction directly into the electrical energy. Among the various next generation power plants, the proton exchange membrane fuel cell (PEMFC) systems has been found to be one of the most promising energy sources due to high efficiency and environment friendly operation [1]. It is important to understand and evaluate the dynamic response of PEMFC systems to current, voltage and power changes for controlling, designing, and optimum operation of the system [2]. As reported in Ref. [3], a FCPP alone may not be sufficient to satisfy all the load demands, especially during peak demand periods or transient events. Over the past few years, various studies performed to understand the dynamic behavior of PEMFCs. For example, Reference [4] discusses the behavior and performance of a PEMFC stack under fast load commutations, and Ref [5] describes a small signal model of the PEMFC. Various studies have been reported in the literature with regard to the dynamic behavior of the PEM fuel cell power plants under various loading conditions. Among them, Benziger et al. investigated the dynamic response of PEM fuel cells to changes in load from a chemical point of view [6]. In Ref. [7], the current distribution and temperature distribution as well as their dynamic changes in fuel cell stack have been evaluated in situ. The information on the internal behavior of three small polymer electrolyte membrane fuel cells under static and dynamic load conditions was extracted in Ref. [8]. Yan et al. investigated the steady state and dynamic performance of PEM fuel cells under various operating conditions and load changes in Ref. [9] using the steady-state polarization curves, transient *I–V* response and electrochemical impedance spectroscopy techniques. However, there is a lack of experimental investigations have been performed to study the dynamic behavior of stand alone FCPPs under sudden load switching and related load conditions such as active-reactive power loading and loads with high harmonic distortion.

It is important to understand FCPP's dynamic behavior in order to estimate the time constants and to understand how a FCPP system with a reformer accommodates transient load conditions. Besides, it is also important to get an insight how the reactive power is supplied in FCPPs and how the inductive loads influence the system. Furthermore, we are also interested to know the dynamic behavior of FCPPs under load conditions consisting of harmonic components.

* Corresponding author. Tel.: +1 251 460 6117; fax: +1 251 460 6028.
E-mail address: malam@usouthal.edu (M.S. Alam).
[1] M. Uzunoglu and O.C. Onar are currently with Yildiz Technical University, 34349 Istanbul, Turkey.

0378-7753/$ – see front matter © 2007 Elsevier B.V. All rights reserved.
doi:10.1016/j.jpowsour.2007.02.045

As FCPPs are expected to be widely used in the near future, voltage stability analysis of these next generation power systems must be considered during planning, operation, and control scenarios. This will ensure that FCPPs will supply more stable, reliable, and high quality energy. Traditional voltage stability analysis can be modified and adapted to the FCPP based power systems.

Voltage stability is associated with the capability of a power system to maintain acceptable voltages under normal and adverse conditions. On the other hand, voltage stability is also defined as the ability of the system to provide adequate reactive power support under both steady-state and transient conditions [10,11]. In voltage stability analysis, load characteristics play an important role [12], and both active and reactive power demand affects system voltage stability [13]. Also, active and reactive power losses increase when an increase in reactive power transfer occurs [13].

To find stability limits via voltage stability analysis, Newton–Raphson approach for power flow analysis may be used. This stability limit, also known as critical point, is often designed as the point where the power flow Jacobian is singular [14] i.e.,

$$\det[J] = 0. \tag{1}$$

A 5 kW FCPP equipped with a battery bank and a power conditioning unit (PCU) is currently operated in authors' laboratory. In this paper, this FCPP is tested under various load conditions in order to obtain the dynamic response of the system. The classified loads are switched for predefined durations when the FCPP is in stand-alone operation mode and the dynamic behavior of the system is observed. Using the experimental results, a validated model has been realized and voltage stability analysis is performed through this model. While experimental results are obtained using Fluke® power analyzers and PlugPower® FCPP system interface, simulation results are obtained using the MATLAB and Simulink software packages.

2. System description and methodology

2.1. Voltage stability analysis

When the Jacobian of Newton–Raphson power flow equations becomes singular, the voltage stability limit i.e., critical point of the system can be determined [15]. The parameters used in the voltage stability analysis are as follows:

V_{ac}	ac output voltage of the inverter [V]
V_L	load terminal voltage [V]
P_L	load active power [W]
Q_L	load reactive power [VAr]
$\delta_{critical}$	critical angle [rad]
$V_{L\text{-critical}}$	critical load voltage [V]
$P_{L\text{-critical}}$	critical load power [W]
X	reactance of the line connecting the combined system [Ω]
δ	phase angle between V_{ac} and V_L [rad]
φ	load phase angle [rad]

The active and reactive power transfer equations can be used to determine the critical parameters for voltage stability analysis

$$P_L = \frac{V_{ac}V_L}{X}\sin\delta, \tag{2}$$

$$Q_L = \frac{V_L^2 - V_{ac}V_L\cos\delta}{X}. \tag{3}$$

The critical values are determined by considering the singularity of the Jacobian matrix using the Newton–Raphson power flow analysis for the two-bus system, expressed as

$$f_1(V_{ac}, V_L, \delta) = P_L - \frac{V_{ac}V_L}{X}\sin\delta, \tag{4}$$

$$f_2(V_{ac}, V_L, \delta) = Q_L - \frac{V_L^2 - V_{ac}V_L\cos\delta}{X}. \tag{5}$$

Eqs. (4) and (5) can be rearranged to form the Jacobian matrix as

$$\begin{bmatrix}\Delta P_L\\ \Delta Q_L\end{bmatrix} = \begin{bmatrix}\frac{\partial f_1}{\partial\delta} & \frac{\partial f_1}{\partial V_L}\\ \frac{\partial f_2}{\partial\delta} & \frac{\partial f_2}{\partial V_L}\end{bmatrix}\begin{bmatrix}\Delta\delta\\ \Delta V\end{bmatrix}. \tag{6}$$

The singularity of the Jacobian matrix may be obtained by setting the determinant of Eq. (6) equal to zero i.e.,

$$\frac{\partial f_1}{\partial\delta}\frac{\partial f_2}{\partial V_L} - \frac{\partial f_2}{\partial\delta}\frac{\partial f_1}{\partial V_L} = 0 \tag{7}$$

and, if we put Eqs. (4) and (5) into Eq. (7) then

$$V_{ac} = 2V_L\cos\delta. \tag{8}$$

Thus, we get the relationship between inverter output and load bus voltages at the critical point. To determine the critical angle, the dependence of V_{ac} and δ is used instead of V_L. The relationship between the real and reactive powers, P_L and Q_L may be expressed as

$$Q_L = P_L\tan\varphi \tag{9}$$

Using Eqs. (2), (3) and (9), the critical angle may be expressed as

$$\tan(2\delta) = \frac{-1}{\tan\varphi} \tag{10}$$

Finally, the critical angle and power values can be obtained from Eqs. (2), (8) (9) and (10) as

$$\delta_{critical} = \frac{1}{2}\arctan\left(\frac{-1}{\tan\varphi}\right) \tag{11}$$

and

$$P_{L-critical} = \frac{V_{ac}^2\tan\delta_{critical}}{2X}, \tag{12}$$

respectively. The phase angle, whose critical value is obtained earlier, depends on the amount of power that the FCPP produces and on some other parameters explained in Section 2.2.

2.2. Mathematical modeling of PEMFC system

The mathematical model parameters of the FC system used in this model are as follows:

B, C	constants to simulate the activation over voltage in PEMFC system and [V]
CV	conversion factor [kmol of hydrogen per kmol of methane]
E	Nernst instantaneous voltage [V]
E_0	standard no load voltage [V]
F	Faraday's constant [C kmol^{-1}]
I_{FC}	FC system feedback current [A]
k_1	PI gain
K_{an}	anode valve constant [$\sqrt{\text{kmol Kg}}$(atm s)$^{-1}$]
K_{H_2}	hydrogen valve molar constant [kmol (atm s)$^{-1}$]
K_{H_2O}	water valve molar constant [kmol (atm s)$^{-1}$]
K_{O_2}	oxygen valve molar constant [kmol (atm s)$^{-1}$]
K_r	modeling constant [kmol (s A)$^{-1}$]
M_{H_2}	molar mass of hydrogen [kg kmol^{-1}]
N_0	number of series fuel cells in the stack
p_{H_2}	hydrogen partial pressure [atm]
p_{H_2O}	water partial pressure [atm]
p_{O_2}	oxygen partial pressure [atm]
q_{H_2}	molar flow of hydrogen [kmol s^{-1}]
q_{O_2}	input molar flow of oxygen [kmol s^{-1}]
$q_{methane}$	methane flow rate [kmol s^{-1}]
$q_{H_2}^{in}$	hydrogen input flow [kmol s^{-1}]
$q_{H_2}^{out}$	hydrogen output flow [kmol s^{-1}]
$q_{H_2}^{r}$	hydrogen flow that reacts [kmol s^{-1}]
$q_{H_2}^{req}$	amount of hydrogen flow required to meet the load change [kmol s^{-1}]
R	universal gas constant [(1 atm) (kmol K)$^{-1}$]
R^{int}	FC internal resistance [Ω]
T	absolute temperature [K]
U	utilization rate
V_{an}	volume of the anode [m^3]
V_{cell}	dc output voltage of FC system [V]
τ_1, τ_2	reformer time constants [s]
τ_3	time constant of the PI controller [s]
τ_{H_2}	hydrogen time constant [s]
τ_{O_2}	oxygen time constant [s]
τ_{H_2O}	water time constant [s]
η_{act}	activation over voltage [V]
η_{ohmic}	ohmic over voltage [V]

The relationship between the molar flow of any gas (hydrogen) through the valve and its partial pressure inside the channel can be expressed as [16]

$$\frac{q_{H_2}}{p_{H_2}} = \frac{K_{an}}{\sqrt{M_{H_2}}} = K_{H_2}. \tag{13}$$

For hydrogen molar flow, three significant factors must be considered—hydrogen input flow, hydrogen output flow, and hydrogen flow during the reaction [16]. The relationship among these factors can be expressed as

$$\frac{d}{dt}p_{H_2} = \frac{RT}{V_{an}}(q_{H_2}^{in} - q_{H_2}^{out} - q_{H_2}^{r}). \tag{14}$$

According to the basic electrochemical relationship between the hydrogen flow and the FC system current, the flow rate of reacted hydrogen is given by [16]

$$q_{H_2}^{r} = \frac{N_0 I_{FC}}{2F} = 2K_r I_{FC}. \tag{15}$$

Using Eqs. (13) and (15), and applying Laplace transform, the hydrogen partial pressure can be obtained in the s domain as [16]

$$p_{H_2} = \frac{1/K_{H_2}}{1 + \tau_{H_2} s}(q_{H_2}^{in} - 2K_r I_{FC}), \tag{16}$$

where

$$\tau_{H_2} = \frac{V_{an}}{K_{H_2} RT}. \tag{17}$$

Similarly, water partial pressure and oxygen partial pressure can be obtained. The polarization curve for the PEMFC is obtained from the sum of the Nernst's voltage, the activation over voltage, and the ohmic over voltage. Assuming constant temperature and oxygen concentration, the FCPP output voltage may be expressed as [3,16,17]

$$V_{cell} = E + \eta_{act} + \eta_{ohmic}, \tag{18}$$

where

$$\eta_{act} = -B \ln (C I_{FC}) \tag{19}$$

and

$$\eta_{ohmic} = -R^{int} I_{FC}. \tag{20}$$

Now, the Nernst's instantaneous voltage may be expressed as [16]

$$E = N_0 \left[E_0 + \frac{RT}{2F} \log \left[\frac{p_{H_2}\sqrt{P_{O_2}}}{p_{H_2O}} \right] \right]. \tag{21}$$

The FCPP consumes hydrogen according to power demand while the reformer continuously generates hydrogen enriched fuel for consumption in the FC stack operation. The reformer model can be expressed as [16,17]

$$\frac{q_{H_2}}{q_{methanol}} = \frac{\text{CV}}{\tau_1 \tau_2 s^2 + (\tau_1 + \tau_2)s + 1}. \tag{22}$$

During operational conditions, to control the hydrogen flow rate according to the output power of the FC system, a proportional-integral (PI) control system is used. To achieve this feedback control, FC current from the output is taken back to the input while converting the hydrogen into molar form [14,17], given by

$$q_{H_2}^{req} = \frac{N_0 I_{FC}}{2FU}. \tag{23}$$

Table 1
The parameters used for the mathematical modeling of the FC system

Specification	Value
Activation voltage constant (B)	0.04777 [A^{-1}]
Activation voltage constant (C)	0.0136 [V]
Conversion factor (CV)	2
Faraday's constant (F)	96484,600 [C $kmol^{-1}$]
FC system internal resistance (R_{int})	No × 0.00303 [Ω]
FC absolute temperature (T)	343 [K]
Hydrogen time constant (τ_{H_2})	3.37 [s]
Hydrogen valve constant (K_{H_2})	4.22×10^{-5} [kmol (s atm)$^{-1}$]
Hydrogen–oxygen flow ratio (r_{H_2O})	1.168
K_r constant = No/4F	2.2802×10^{-7} [kmol (s A)$^{-1}$]
Line reactance (X)	0.0809 [Ω]
Methane reference signal ($Q_{methref}$)	0.000015 [kmol s^{-1}]
No load voltage (Eo)	0.8 [V]
Number of cells (No)	88
Number of stacks (N_S)	1
Oxygen time constant (τ_{O_2})	6.74 [s]
Oxygen valve constant, (K_{O_2})	2.11×10^{-5} [kmol (s atm)$^{-1}$]
PI gain constant (k_1)	0.25
Reformer time constant (τ_1, τ_2, τ_3)	2 [s]
Universal gas constant (R)	8314.47 [J (kmol K)$^{-1}$]
Utilization factor (U)	0.8
Water time constant (τ_{H_2O})	18.418 [s]
Water valve constant (K_{H_2O})	7.716×10^{-6} [kmol (s atm)$^{-1}$]

The amount of hydrogen available from the reformer can be used to control the methane flow rate by using a PI controller [16,17], expressed as

$$q_{\text{methane}} = \left(k_1 + \frac{k_1}{\tau_3 s}\right)\left(\frac{N_0 I_{\text{FC}}}{2FU} - q_{\text{H}_2}^{\text{in}}\right). \tag{24}$$

The mathematical model of the FC system can be obtained using the above equations. The parameters for the mathematical modeling of the FC system are given in Table 1.

2.3. Power conditioning unit (PCU)

The FCPP produces dc electrical energy which must be converted to ac electrical energy for household appliances. The considered system for domestic loads requires a dc/ac inverter, which also acts as an energy management unit to match the different dynamics of the FC system, battery bank and various types of loads.

The parameters used in the mathematical modeling of the PCU in the mathematical model are as follows:

I_{battery} battery bank current [A]
I_{dc} dc current [A]
I_{FC} FC system current transferred to dc bus [A]
I_{L} load current [A]
m inverter modulation index
P_{ac} ac output power [W]
P_{L} load power [W]
V_{ac} ac output voltage of the inverter [V]
V_{dc} combined system dc terminal voltage [V]
V_{r} reference voltage signal [V]
V_{L} load terminal voltage [V]
X reactance of the line connecting the FC system and the load [Ω]
θ load phase angle [rad]

The ac voltage and active power at the inverter output can be expressed as a function of the modulation index and phase angle as [16]

$$P_{\text{ac}} = \frac{m V_{\text{dc}} V_{\text{L}}}{X} \sin(\delta). \tag{25}$$

The corresponding load current and dc current can be expressed as

$$I_L = \frac{P_L}{V_L \cos(\theta)}, \tag{26}$$

$$I_{\text{dc}} = m I_{\text{L}} \cos(\theta + \delta), \tag{27}$$

Assuming a lossless inverter, P_{ac} can be expressed as [16]

$$P_{\text{ac}} = P_{\text{dc}} = V_{\text{dc}} I_{\text{dc}}. \tag{28}$$

According to Eq. (23), the amount of required hydrogen flow can be calculated as

$$q_{\text{H}_2}^{\text{req}} = \frac{N_0(I_{\text{dc}} + I_{\text{battery}})}{2FU}. \tag{29}$$

If the battery bank is discharging, the current is negative. If the battery bank is charging, the current is positive. According to Eqs. (2), (28) and (29) the variation of the phase angle δ can be obtained as

$$\delta = \sin^{-1}\left(\frac{((2q_{\text{H}_2} FU/N_0) + I_{\text{battery}})\, X}{m V_{\text{L}}}\right). \tag{30}$$

2.4. Experimental setup

The 5 kW PEMFC system currently operated in our laboratory feeds a 500-square-foot house as shown in Fig. 1. The FCPP can be operated in the stand-alone or in the grid parallel mode. In this study, experimental results are obtained when the FCPP was operated in the stand-alone mode.

This FCPP's PCU consists of an inverter, dc/dc converters and a battery bank. The PCU supplies power to internal auxiliary components of the FC system, manages charging and discharging of the battery bank, and supplies the load requirements. There are four, 12-V maintenance-free lead-acid batteries integrated in series to the inverter. The battery bank supplies auxiliary power during cold-start of the FCPP, and supports peak demand periods or transient events and compensates the tracking delays of the FC stack power.

To observe the dynamic behavior of the FCPP and the effects of various loads on system voltage stability, the following types of loads were used:

- Resistive loads,
- Inductive loads,
- Resistive-inductive loads,
- Loads with high harmonic distortion.

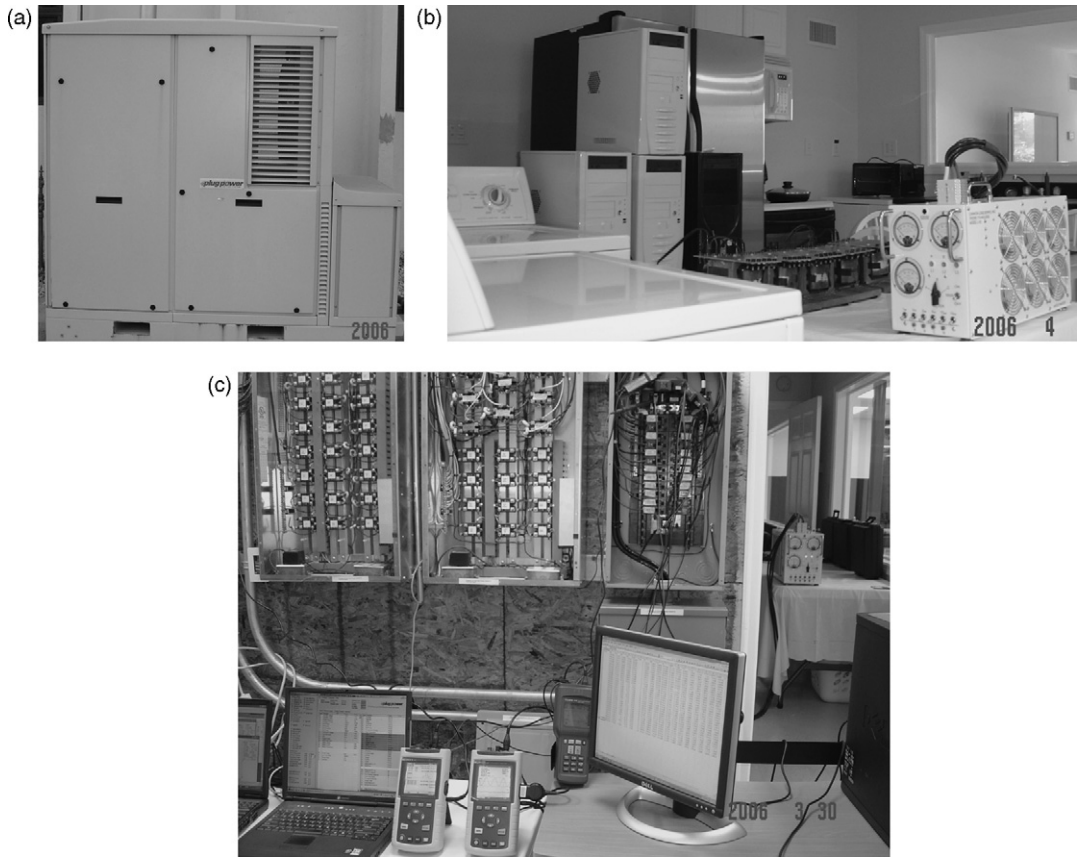

Fig. 1. Test experimental setup: (a) FC system, (b) various loads and (c) measurement systems.

The specific types of loads and the corresponding switching intervals are shown in detail in Table 2. Experimental results are obtained for the time interval between 04:02:20 P.M. and 04:49:00 P.M. of the recorded data. This time interval corresponds to the 2800 s of duration. The chosen loads are switched according to the given order and all results are obtained according to the load types and time durations given in Table 2.

The ac load bus quantities are measured using Fluke power analyzers while the quantities related to FCPP, PCU and battery bank are measured using PlugPower FC system interface software. All data measurement and logging devices are synchronized. At first, the FCPP was switched to stand-alone operation mode under a base load and the data logging procedure is started at $t = 0$. After 70 s, classified loads were switched on according to the sequence and durations given in Table 2.

Table 2
Various loads used in the experimental study

Loads	Time intervals (s)
Washing machine	[70–259], [1134–1328] and [1338–1535]
Microwave	[266–332] and [339–466]
4 × Computer (without monitors)	[479–719], [950–1128] and [1338–1535]
4 × Small transformers (secondary open-circuited)	[735–1985]
1 × Small transformer (secondary open-circuited)	[1841–1985]
2 × Small transformers (secondary open-circuited)	[1986–2105]
Resistive load bank (switch 1)	[2113–2417] and [2608–2757]
Resistive load bank (switch 2)	[2418–2607]

3. Results and discussions

The block diagram of the integrated overall system is shown in Fig. 2.

Figs. 3–8 show the results for the ac bus measurements involving active power, reactive power, power factor, load voltage and total harmonic distortion (THD) of voltage and current, respectively.

Figs. 3 and 4 show that there is a constant active and reactive power values of 130 W and 120 VAr because of the control and measurement devices connected to the ac side. The active and reactive power variations above these values are caused by the loads as given in Table 2. The load variations switched as shown in Table 2 was selected to build a variety of active and reactive loading combinations to test the PEMFC power plant under these conditions. Thus, we could observe the dynamic performance of the plant under different power factor values as shown in Figs. 3 and 4. According to the Figs. 3 and 4, resistive load bank draws mostly active power while transformers draw mostly reactive power. The washing machine and microwave draw both active and reactive power.

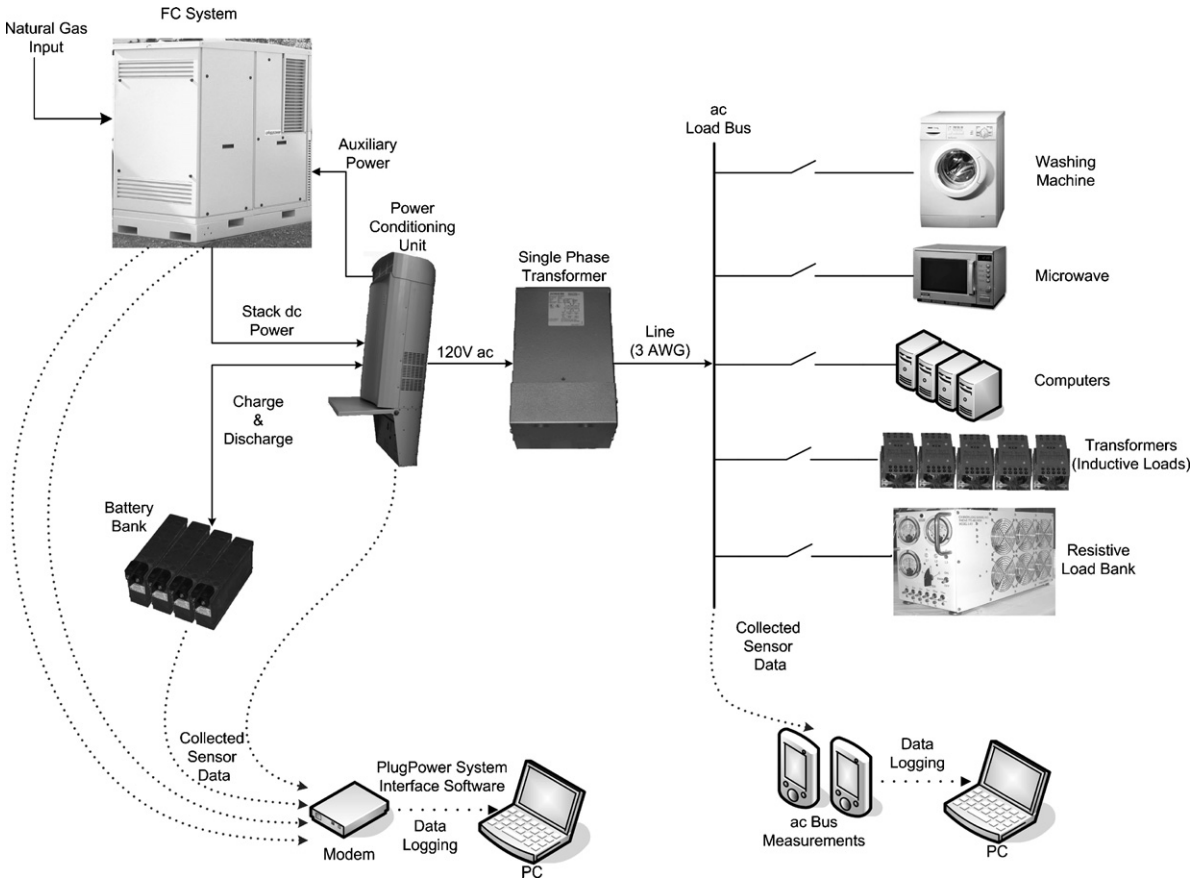

Fig. 2. The overall system block diagram.

From Fig. 5, we observe that the load bus voltage varies according to the load power which causes voltage drop on the equivalent system impedance between the inverter output and load buses. The reactive power oscillates between the inverter output and the load bus, thus reactive power demand can be met as a result of the voltage variations shown in Fig. 5. The ac load bus voltage oscillates between the 112.2 V minimum and 116.8 V maximum.

Nonlinear elements generally cause harmonics which result in current and voltage distortions in electrical systems. A measure of the distortion is represented by the ratio of the equivalent harmonics to the percentage of the fundamental signal amplitude which is well known as THD. The THD of the voltage and current distortions are given in Figs. 6 and 7 respectively, when the loads were turned on in predefined time intervals. In particular, the microwave and computers have the highest harmonic

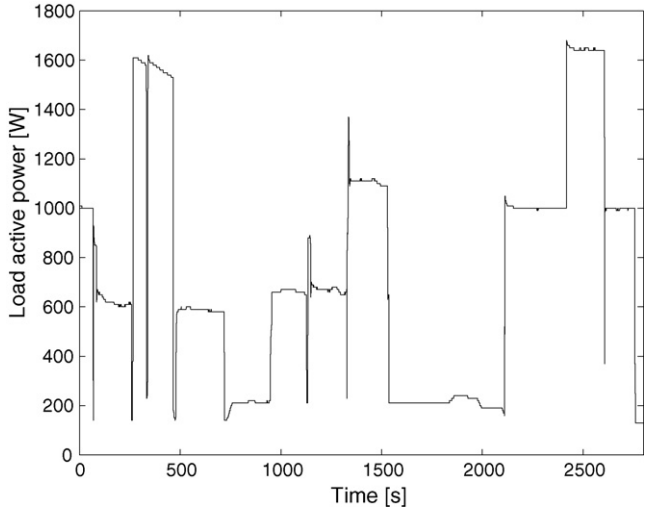

Fig. 3. ac load bus active power variation under various load conditions.

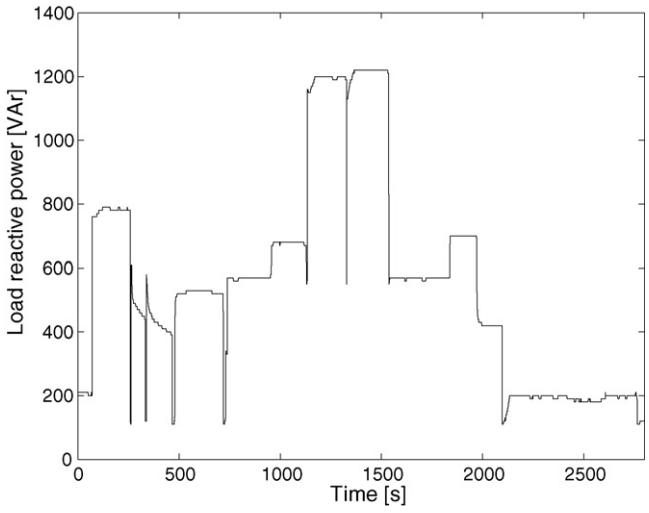

Fig. 4. ac load bus reactive power variation under various load conditions.

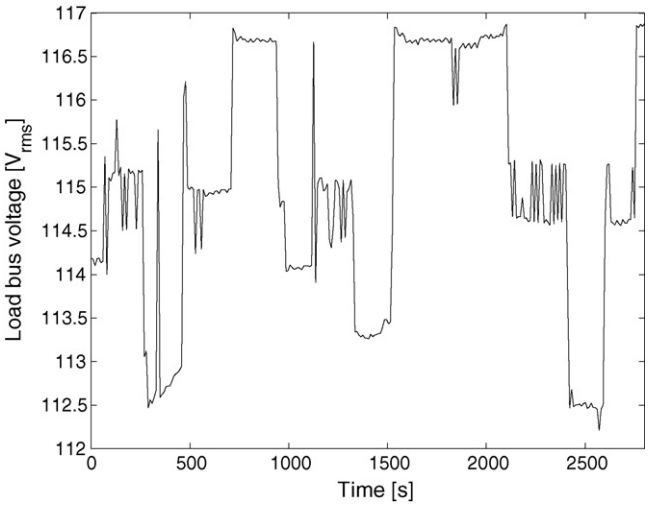

Fig. 5. ac load bus voltage variation under various load conditions.

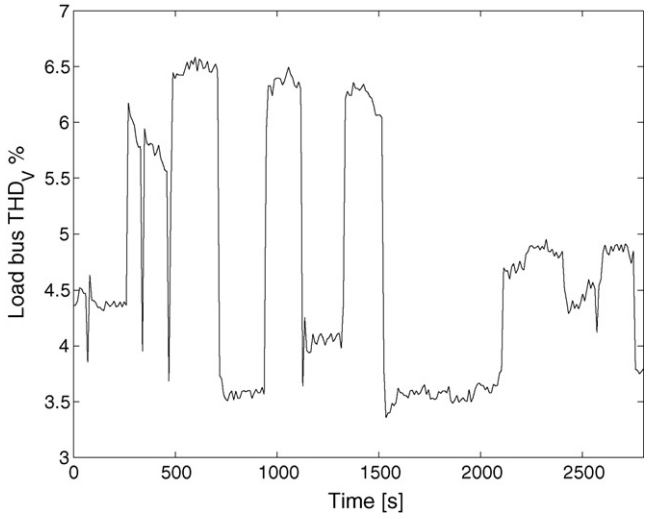

Fig. 6. ac load bus total harmonic distortion for voltage variation under various load conditions.

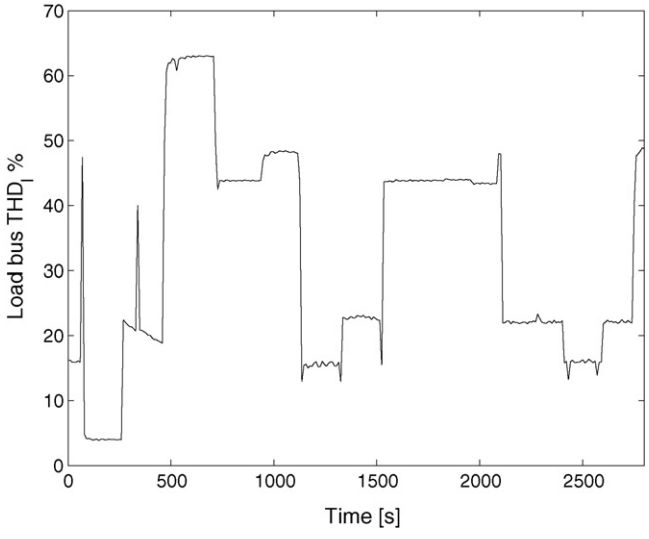

Fig. 7. ac load bus total harmonic distortion for current variation under various load conditions.

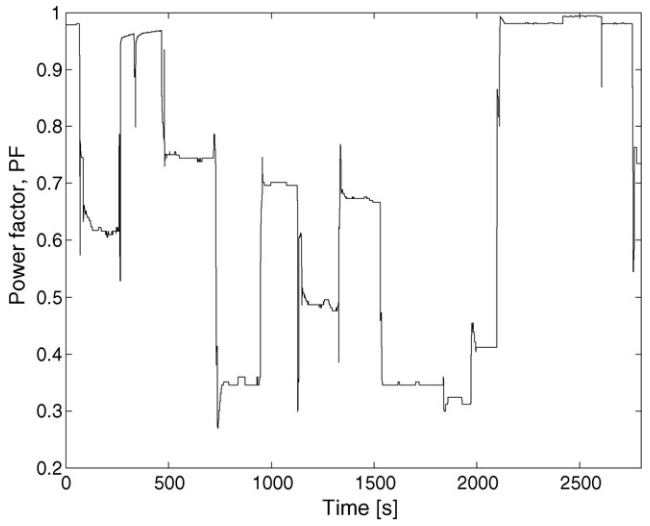

Fig. 8. ac load bus power factor (PF) variation under various load conditions.

distortions since they have power electronic circuits. The THD affects the power factor (PF) which considers the fundamental and harmonic components while traditional cosφ considers the fundamental component only. The variation of the PF is shown in Fig. 8.

Figs. 9–15 show the results related to the FCPP, battery and PCU outputs, stack dc power, cell and stack voltages, battery power, inverter output voltage and current, average ac power and phase angle, respectively.

To meet the required load power, FCPP produces the stack dc power shown in Fig. 9. This produced power includes the auxiliary power, charging power of the battery, and the power transferred to the dc bus. The FC stack produces dc power to track the active power demand of the load as depicted in Fig. 3. According to the Fig. 9, we can mention that the stack dc power follows the general trend of the active load demand. However, it does not match the demand at all because it has step-up and step-down time delays. The reasons of these mismatches are caused

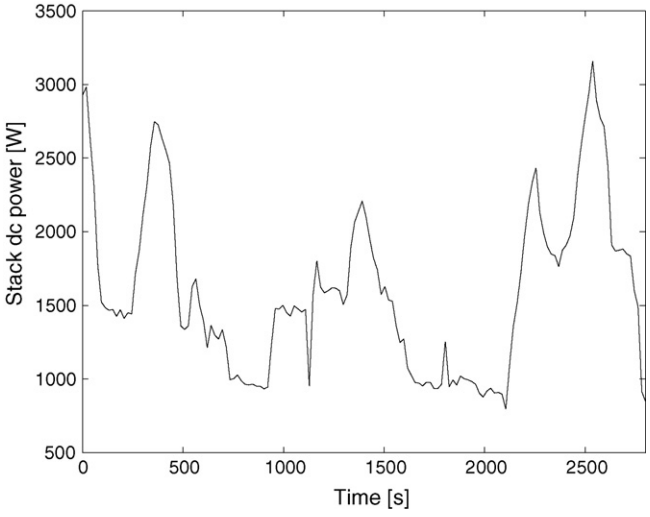

Fig. 9. The variation of FC stack dc power according to load demand.

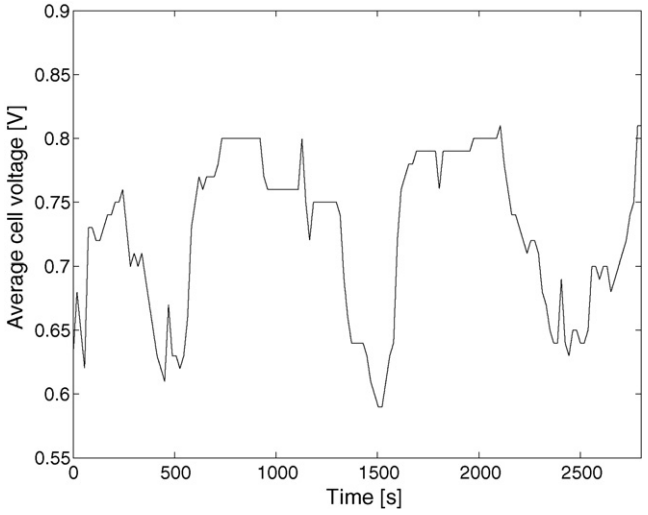

Fig. 10. The average cell voltage according to load demand.

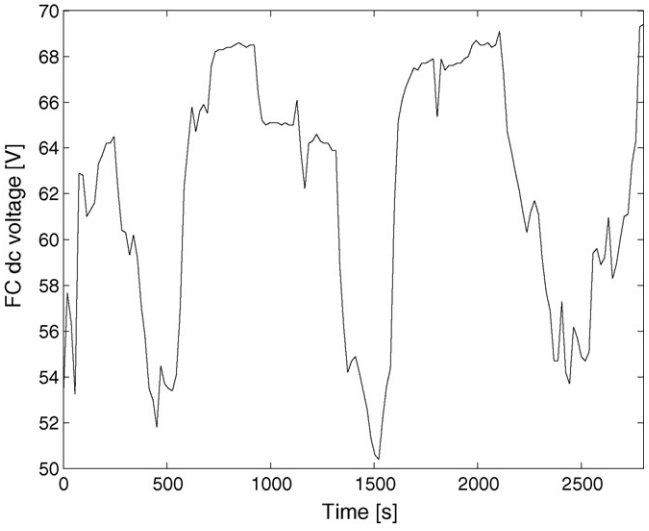

Fig. 11. The FC system voltage according to load demand.

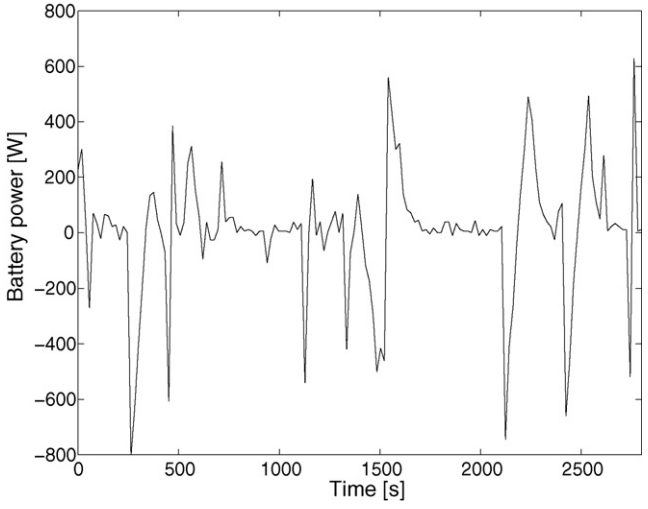

Fig. 12. Battery power including charges and discharges.

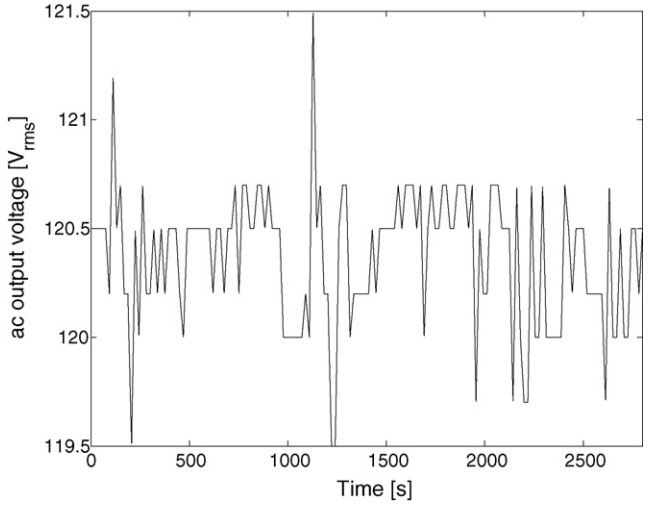

Fig. 13. The variation of inverter output voltage.

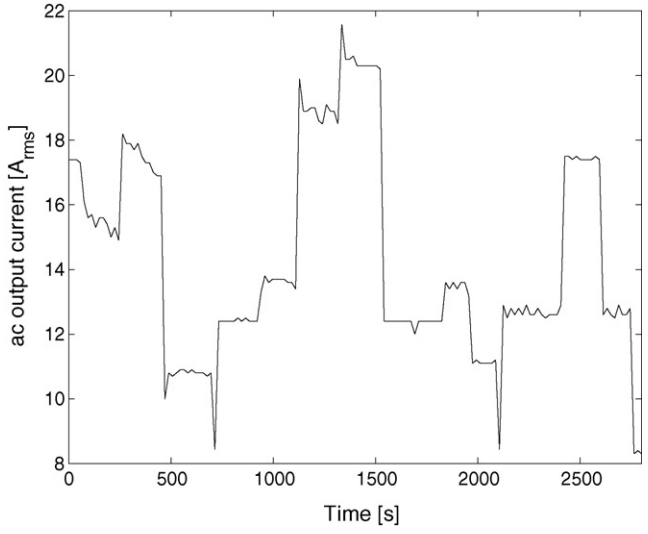

Fig. 14. The variation of inverter output current.

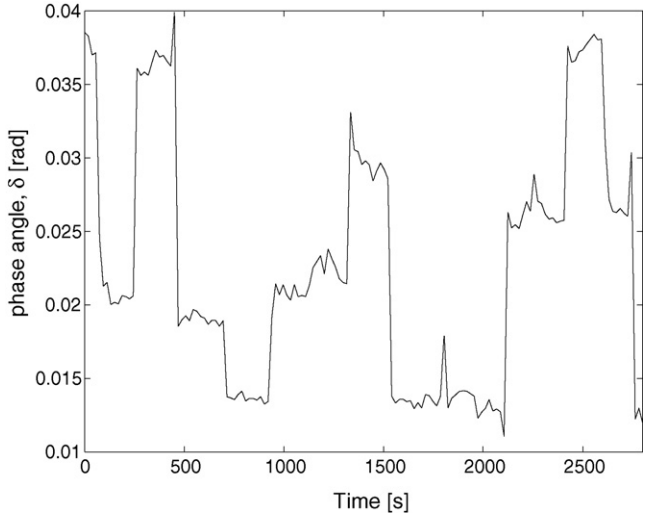

Fig. 15. The variation of ac voltage phase angle.

by the time constants of the fuel cell dynamics, particularly the time constants of the reformer dynamics.

The response of the cell and stack voltages varies as shown in Figs. 10 and 11, respectively, according to the amount of power supplied by the FC system as shown in Fig. 9. The stack dc voltage and average cell voltage decrease when the FC output power increases due to the FC power–voltage relationship. The stack dc voltage varies according to the active and reactive powers drawn from the fuel cell. From Figs. 9–11, it is obvious that the PEMFC stack equipped with reformer has a slow dynamic response.

The stack dc power given in Fig. 9 is insufficient to meet the load power requirements. It is obvious that the stack power only tracks the general trend of the power demand, and needs further conditioning to match the actual load demand. From Fig. 12, it is seen that the battery bank supplies the power to compensate all mismatches and tracking delays between the load and the stack powers by charging and discharging. Additionally, the battery bank assists FC during peak demand periods and transient events. Without a storage device as an auxiliary power source, the FC power plant would have to supply all power demand thus increasing the size and cost of the FC power plant. The battery power becomes negative when it supplies power to the dc bus, and it becomes positive when it is recharged. The PCU uses stack and battery power to condition the output ac power.

The inverter output voltage is successfully controlled by the PCU within the acceptable limits as illustrated in Fig. 13. However, the most significant deviations of the ac output voltage (although it is not very high) is recorded when the loads including reactive components such as washing machine and small transformers are switched on. It may be mentioned that the magnitude of the voltage oscillations increases during the reactive load switching. However, the inverter keeps its output voltage within acceptable limits from minimum 119.5 V to maximum 121.5 V while tracking the reference voltage.

According to the inverter output active power (Fig. 3), reactive power (Fig. 4) and voltage (Fig. 13), the ac output current varies as given in Fig. 14. This current profile consists of active and reactive load currents.

We also observe that this apparent current influences average cell and stack voltages given in Figs. 10 and 11, respectively. An increase in reactive power demand causes a proportional decrease in the FCPP output voltage. Although the fuel cell is a dc source, the resultant current of active and reactive current components has an effect on average dc cell voltage and stack dc voltage which is an interesting result obtained in this experimental study.

The variation of δ is depicted in Fig. 15 which can be attained using the parameters given in Eq. (30). The parameters of Eq. (30) are obtained using the experimental data and mathematical modeling. From Fig. 15, we can observe that the phase angle δ varies with respect to the active load demand from the fuel cell stack and it tracks the general trend of the active load variation.

Figs. 16–19 show the results of critical angle and power at the load bus. The variations of critical values are produced experimentally through mathematical modeling to account for the parameters given in Eqs. (11) and (12).

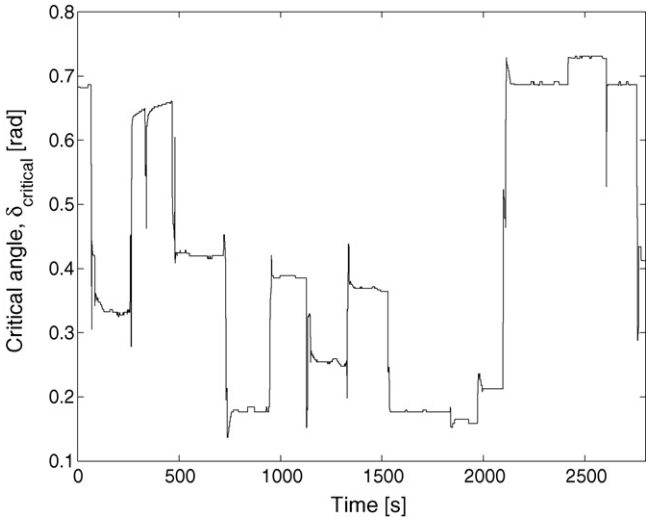

Fig. 16. The variation of critical angle at the load bus.

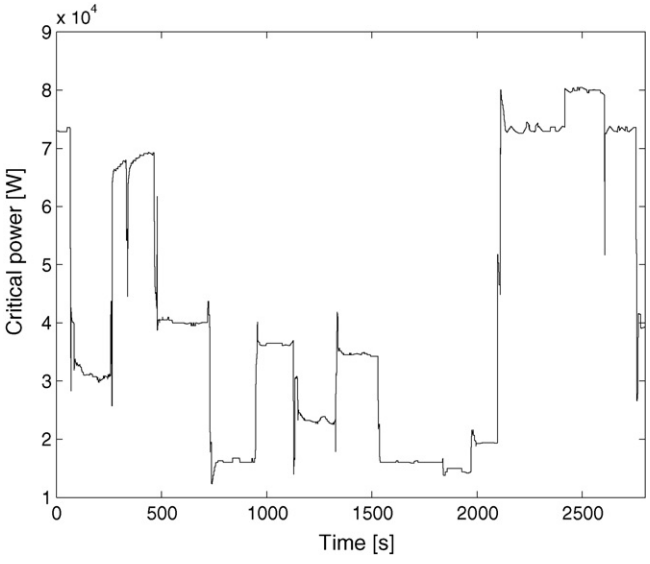

Fig. 17. The variation of critical power at the load bus.

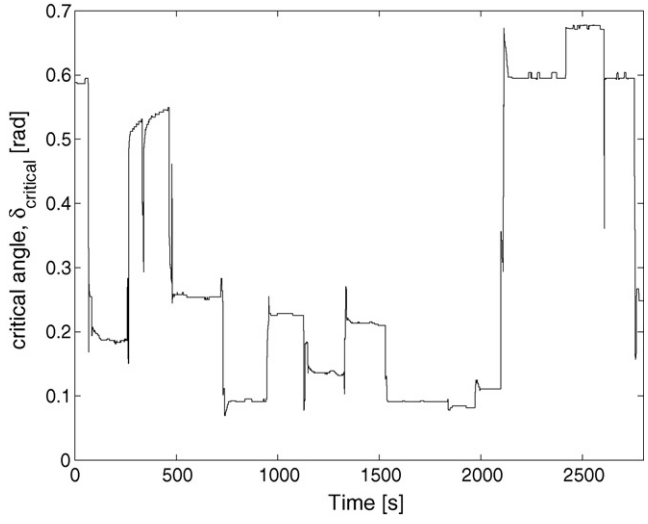

Fig. 18. The variation of critical angle at the load bus.

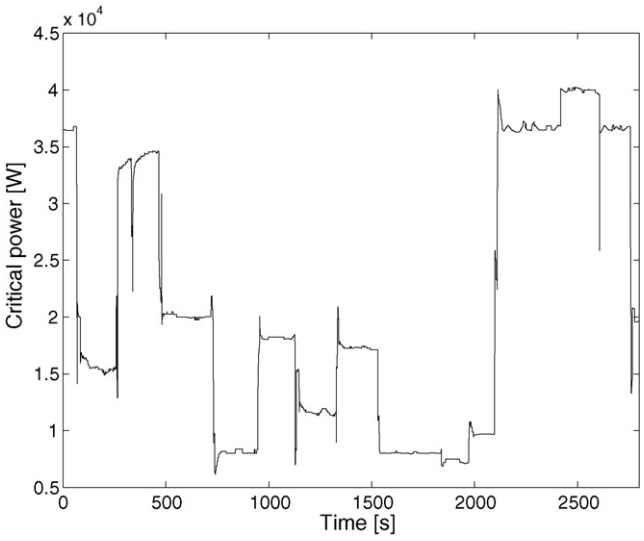

Fig. 19. The variation of critical power at the load bus.

The variation of critical phase angle is given in Fig. 16. It is seen that the critical angle varies according to the power factor. All parameters which affect the power factor have an effect on the critical angle as well. Fig. 17 shows the variation of critical active power which is affected by the critical angle (δ_{critical}), ac voltage and equivalent reactance of the line connecting the FCPP to the load. The critical angle and the critical power can also be called as the stability margins of the system. If we get closer to these critical values in any loading condition, the system will be very risky in terms of stable and safe operation. The voltage stability may be disturbed and voltage collapses may occur if these limits get enforced.

Two of the above mentioned parameters are tested separately to ascertain how they affect the voltage stability. One of the parameters is the amount of reactive power drawn from the FCPP and the other is the reactance of the line connecting the FCPP to the load. At first, the reactive power is assumed to be two times greater then the original demand and then, the variation of new critical angle is given in Fig. 18. Then the line reactance is assumed to be two times greater than the original value and the variation of new critical power is given in Fig. 19. From Figs. 18 and 19, it is evident that the increase in either the reactive power or the line reactance, results in a decrease in the critical power and critical angle. Thus, the system gets closer to the risky operating points in terms of voltage stability.

4. Conclusions

In this paper, the dynamic behavior of the FCPP is tested under various loads and their effects on voltage stability are analyzed using a PEMFC based power system. Based on the analysis and experimental results, we can conclude the following:

- Due to the slow dynamic response of the tested FC stack equipped with a reformer, FCPP needs an auxiliary energy storage system. The FCPP needs to be integrated with extra energy storage devices such as battery or ultra-capacitor bank to successfully meet all load demands.
- Battery bank assists FCPPs during transient and peak demand periods, and tries to prevent the power tracking delays and mismatches.
- To meet the reactive power demand results in voltage drop at the load bus. Both the active power and the reactive power demand influences the inverter output voltage, average cell voltage and stack voltage.
- The power factor decreases due to the harmonic reactive powers drawn by the nonlinear elements. Furthermore, it may be mentioned that the higher harmonic distortion negatively affects stability.

From the voltage stability analysis, it is evident that the power and phase angle values do not reach the critical values in the current scenario. However, for different applications, the critical values must be considered in order to maintain the voltage stability. For systems with long line distances and/or high reactive power requirements, the stability analysis should be performed prior to the design and operation of FCPPs.

Acknowledgements

This work was supported in part by the U.S. Department of Energy under Grant DE-FG02-05CH11295.

References

[1] L. Gao, Z. Jiang, R.A. Dougal, An actively controlled fuel cell/battery hybrid to meet pulsed power demands, J. Power Sources 130 (1–2) (2004) 202–207.
[2] S. Kim, S. Shimpalee, J.W. Van Zee, The effect of stoichiometry on dynamic behavior of a proton exchange membrane fuel cell (PEMFC) during load change, J. Power Source 135 (1–2) (2004) 110–121.
[3] M. Uzunoglu, M.S. Alam, Dynamic modeling, design and simulation of a combined PEM fuel cell and ultra-capacitor system for stand alone residential applications, IEEE Trans. Energy Convers. 21 (3) (2006) 767–775.
[4] J. Hamelin, K. Agbossou, A. Laperriere, F. Laurencelle, T.K. Bose, Dynamic behavior of a PEM fuel cell stack for stationary applications, Int. J. Hydrogen Energy 26 (1) (2001) 625–629.
[5] L.Y. Chiu, B. Diong, R.S. Gemmen, An improved small-signal model of the dynamic behavior of PEM fuel cells, IEEE Trans. Ind. Appl. 40 (4) (2004) 970–977.
[6] J. Benziger, E. Chia, J.F. Moxley, I.G. Kevrekidis, The dynamic response of PEM fuel cells to changes in load, Chem. Eng. Sci. 60 (6) (2005) 1743–1759.
[7] X. Yan, M. Hou, L. Sun, H. Cheng, Y. Hong, D. Liang, Q. Shen, P. Ming, B. Yi, The study on transient characteristics of proton exchange membrane fuel cell stack during dynamic loading, J. Power Sources 163 (2) (2007) 966–970.
[8] R.A. Costa, J.R. Camacho, The dynamic and steady state behavior of a PEM fuel cell as an electric energy source, J. Power Sources 161 (2) (2006) 1176–1182.
[9] Q. Yan, H. Toghiani, H. Causey, Steady state and dynamic performance of proton exchange membrane fuel cells (PEMFCs) under various operating conditions and load changes, J. Power Sources 161 (1) (2006) 492–502.
[10] C.S. Indulkar, B. Viswanathan, S.S. Venkata, Maximum power transfer limited by voltage stability in series and shunt compensated schemes for AC transmission systems, IEEE Trans. Power Deliv. 4 (2) (1989) 1246–1252.

[11] M. Uzunoglu, Harmonics and voltage stability analysis in power systems including thyristor-controlled reactor, Acad. Proc. Eng. Sci.-Sadhana 30 (1) (2005) 57–67.
[12] M.K. Pal, Voltage stability conditions considering load characteristics, IEEE Trans. Power Syst. 7 (1) (1992) 243–249.
[13] P. Kundur, Power System Stability and Control, McGraw-Hill, New-York, 1994.
[14] N. Yorino, H. Sasaki, Y. Masuda, Y. Tamura, M. Kitagawa, A. Oshima, An Investigation of Voltage instability problems, IEEE Trans. Power Syst. 7 (2) (1992) 600–611.
[15] M. Uzunoglu, C. Kocatepe, R. Yumurtaci, Voltage-stability analysis in power systems including non-linear loads, Eur. Trans. Electr. Power 14 (1) (2004) 41–56.
[16] M.Y. El-Sharkh, A. Rahman, M.S. Alam, P.C. Byrne, A.A. Sakla, T. Thomas, A dynamic model for a stand-alone PEM fuel cell power plant for residential applications, J. Power Sources 138 (1–2) (2004) 199–204.
[17] K.-H. Hauer, "Analysis tool for fuel cell vehicle hardware and software (controls) with an application to fuel economy comparisons of alternative system designs," Ph.D. dissertation, Dept. Transportation Technology and Policy, University of California Davis,. (2001).